Synthesis, crystal structures and optical properties of open-framework gallium phosphates: $NaGa_3F_4(PO_4)_2(H_2O)_2$ and $AGa_2P_2O_7(OH)_3(H_2O)$ (A = K, Rb)

Tianyou Wang,[a] Chao Wu,[a] Lin Lin,[a] Zhipeng Huang,[a] Mark G. Humphrey,[b] Chi Zhang[a,*]

[a] China-Australia Joint Research Center for Functional Molecular Materials, School of Chemical Science and Engineering, Tongji University, Shanghai 200092, P. R. China

[b] Research School of Chemistry, Australian National University, Canberra, ACT 2601, Australia

*Correspondence: E-mail: chizhang@tongji.edu.cn; Phone: (+86)21-65988860.

Abstract: Three new alkali-metal gallium phosphates $NaGa_3(PO_4)_2F_4(H_2O)_2$ (**1**), $KGa_2P_2O_7(OH)_3(H_2O)$ (**2**), and $RbGa_2P_2O_7(OH)_3(H_2O)$ (**3**) were obtained using hydrothermal methods. Compound **1** crystallizes in the chiral space group $P4_32_12$. The structure of **1** features a three-dimensional (3D) framework composed of 2D layers of corner-sharing GaO_4F_2 and GaO_2F_4 octahedra that are further bridged by PO_4 tetrahedra with Na^+ cations residing in the oxyfluorinated gallolayers. Compounds **2** and **3** are isostructural, both crystallizing in the centrosymmetric space group $P2_1/c$; their structures consist of novel 3D gallophosphate frameworks constructed from Ga_4O_{20} tetramers interconnected by PO_4 units with 8-membered ring channels along the *b*-axis, in which K^+/Rb^+ cations are located. The diffuse reflectance spectra show that the ultraviolet (UV) cut-off edges are about 292 nm (4.25 eV), 275 nm (4.51 eV) and 306 nm (4.05 eV) for **1**−**3**, respectively. Luminescent studies suggest that **1**−**3** emit blue light under the excitation of near-ultraviolet light.

Keywords: Hydrothermal reaction; Crystal structures; Open-framework; Phosphates; Luminescent

1 INTRODUCTION

Metal phosphates have attracted considerable interest because of their abundant structural chemistry [1] and their potential applications such as solid electrolytes [2], luminescent hosts [3], nonlinear optical (NLO) materials [4] and magnetism [5]. These wide applications mainly originate from the diverse porous or polar structures of metal phosphates. As a polarizable fundamental building unit (FBU), the PO_4 tetrahedra favor condensation to form different types of P_xO_y groups exemplified by P_2O_7 (pyrophosphates), P_nO_{3n+1} clusters, P_nO_{3n} cyclic rings or infinite $(PO_3)_\infty$ chains ($n \geq 3$, polyphosphates) [6,7].

Metal gallium phosphates constitute an important family of metal phosphates, which exhibits a rich structural and compositional diversity because of the flexible coordination environments of metal gallium (GaO_4 tetrahedra, GaO_5 trigonal bipyramids, and GaO_6 octahedra) [8]. During the last decades, a large number of gallium phosphates with one dimensional (1D) chains, 2D sheets, and 3D open frameworks have been reported [9]. In order to pursuit widespread use of gallium phosphates as ion-exchange, catalytic and optical materials, incorporation of hetero-metals into their frameworks has been attempted, which may lead to the modification of physical or chemical properties [10]. The presence of alkali metals usually gives rise to rather dense architectures, such as $NaGa_2(OH)(PO_4)_2$ [11], $Rb_2[Ga_4(HPO_4)(PO_4)_4]\cdot 0.5H_2O$ [12], $Cs_2Ga_6(OH)_2(PO_4)_6$ [13], $LiGa(OH)PO_4$ [14], $RbGa_3(P_3O_{10})_2$ [15], and $K[(GaPO_4)\{F_{1/4}(GaPO_4)\}_4]$ [16]. Additionally, the

incorporation of fluorine into inorganic framework structures often changes the structures and compositions of the compounds because of its high electronegativity which not only gives rise to the cut-off edge shift towards the blue wavelength but also helps to increase the thermal stability [17]. Many efforts have been devoted to searching for new fluorophosphates with NLO, electrochemical and luminescent properties [18]. However, it is rarely reported about pure inorganic gallium fluorophosphates as luminescent materials [18c,19].

Several different approaches have been employed to synthesize phosphates. High-temperature solid-state reactions have afforded a wide variety of metal phosphates with high thermal stabilities and strong luminescence intensities [20]; although the high-temperature procedure can produce well-defined crystals, it requires lengthy reactions and often forms glassy products [21]. Hydrothermal methods have proven to be successful, affording a variety of crystalline phosphates materials, such as $[Zn_2(bip)(HPO_4)_2]\cdot 2H_2O$ [22], $(NH_4)_{1-2x}Mn_{1+x}(H_2O)_2(BP_2O_8)\cdot yH_2O$ [23], $(HDADD)_2(BPDC)_{0.5}[Ga_3(OH)_2(HPO_4)_4]$ [24], $K_4Mg_4(P_2O_7)_3$ [25], Cs_2LiPO_4 [26], and $(NH_4)_2PO_3F$ [27], which have also attracted great attention owing to their varying structural characteristics and interesting optical properties. Among them, a large number of phosphates with acentric structures display excellent NLO performance and some zinc and gallium phosphates with extra large channel structures can emit blue light or can even synchronize dual wavelengths (blue and yellow) to give out white light under the excitation of ultraviolet (UV) light [22-28]. In contrast to the

other heterometallic phosphates, the synthesis of alkali-metal gallium phosphates under facile hydrothermal conditions is less explored [29].

We report herein the synthesis of three open-framework alkali-metal gallium phosphates $NaGa_3(PO_4)_2F_4(H_2O)_2$ (**1**), $KGa_2P_2O_7(OH)_3(H_2O)$ (**2**), and $RbGa_2P_2O_7(OH)_3(H_2O)$ (**3**) via straight-forward hydrothermal methods. The crystal structures, thermal stabilities, IR spectra, SHG measurements, UV-Vis-NIR diffuse reflectance spectra, and luminescent properties with a short cut-off edge and blue light-emitted for compounds **1**−**3** are also described in this paper.

2 EXPERIMENTAL SECTION

2.1 Reagents. GaO(OH) (99%, Xiya Reagent), NaF (99.8%, Adamas Reagent), KCl (99.5%, Adamas Reagent), RbCl (99.95%, Adamas Reagent), H_3PO_4 (99.5%, Adamas Reagent) and $(NH_4)(H_2PO_4)$ (99.5%, Adamas Reagent), HF (40%, Adamas Reagent) were obtained commercially and used as received.

2.2 Synthesis of $NaGa_3(PO_4)_2F_4(H_2O)_2$ (1). A mixture of GaO(OH) (0.35 g, 3.4 mmol), NaF (0.293 g, 7 mmol), H_3PO_4 (0.5 mL), 40% HF (0.25 mL), and deionized water (4 mL) was sealed in a 20 mL autoclave with a Teflon liner. The autoclave was heated at 180 ºC for 72 h, and then slowly cooled to 30 ºC at 3.5 ºC/h. Colorless block crystals of **1** were collected and dried in air. Yield: 48% (0.29 g, based on Ga). IR data (KBr pellet, cm^{-1}): 3490 (br, m), 1640 m, 1061 s, 575 m.

2.3 Synthesis of $KGa_2P_2O_7(OH)_3(H_2O)$ (2). A mixture of GaO(OH) (0.205 g, 2 mmol), KCl (0.447 g, 6 mmol), $(NH_4)(H_2PO_4)$ (0.230 g, 2 mmol), and H_2O (4 mL)

was sealed in a 20 mL autoclave equipped with a Teflon liner. The autoclave was heated at 180 ºC for 72 h, and then slowly cooled to 30 ºC at 4 ºC/h. After washing with deionized water, colorless block crystals of **2** were isolated using a microscope (0.21 g, 50% based on Ga). IR data (KBr pellet, cm^{-1}): 3457 m, 3325 m, 1654 w, 1101 s, 1003 s, 601 m, 560 m.

2.4 Synthesis of $RbGa_2P_2O_7(OH)_3(H_2O)$ (3). The same procedure was employed to synthesize **2** except using RbCl (0.725 g, 6.00 mmol) instead of KCl. Colorless block crystals of $RbGa_2P_2O_7(OH)_3(H_2O)$ (**3**) were obtained (0.20 g, 43% based on Ga). IR data (KBr, cm^{-1}): 3475 m, 3364 m, 1654 w, 1101 s, 996 s, 621 m, 561 m.

2.5 Structural Determination. Single-crystal X-ray diffraction data of **1**−**3** were collected at room temperature on a Bruker D8 VENTURE CMOS X-ray diffractometer using graphite-monochromated Mo-Kα radiation (λ = 0.71073 Å). APEX II software was applied to collect and reduce data. Semi-empirical absorption corrections based on equivalent reflections were applied for both data sets using the APEX II program. The three structures were solved by direct methods and refined on F^2 by full-matrix least-squares methods using SHELXTL [30]. All non-hydrogen atoms were refined anisotropically. Oxygen atoms that assigned as hydroxyl groups and water molecules were refined on the basis of the requirements of charge balance and bond valence calculations. All three structures were checked with PLATON, and no other higher symmetry elements were found [31]. Table 1 summarizes the crystal data and structural refinement parameters for the three compounds. Selected bond

distances (Å) and angles (deg) are collected in Table S1−S3 (Supporting Information).

Table 1 Crystallographic Data and Structure Refinement Parameters for **1**−**3**.[a]

Empirical formula	$NaGa_3F_4(PO_4)_2(H_2O)_2$	$KGa_2P_2O_7(OH)_3(H_2O)$	$RbGa_2P_2O_7(OH)_3(H_2O)$
Formula weight	534.12	421.52	467.89
Temperature (K)	293(2)	293(2)	293(2)
Crystal system	tetragonal	monoclinic	monoclinic
Space group	$P4_32_12$	$P2_1/c$	$P2_1/c$
a (Å)	7.1707(2)	9.6213(4)	9.6583(8)
b (Å)	7.1707(2)	9.5651(3)	9.6224(9)
c (Å)	19.2172(12)	12.0512(3)	12.1271(8)
α (˚)	90	90	90
β (˚)	90	128.528(2)	128.474(4)
γ (˚)	90	90	90
V (Å^3)	988.13(7)	867.62(5)	882.35(12)
Z	4	4	4
D_{calc} (g·cm^{-3})	3.590	3.227	3.522
μ (mm^{-1})	8.610	7.114	12.005
F(000)	1016	816	888
θ range (˚)	3.03-26.36	3.03-26.48	3.01-26.39
Limiting indices	-8 ≤ h ≤ 8, -8 ≤ k ≤ 8, -24 ≤ l ≤ 23	-11 ≤ h ≤ 11, -11 ≤ k ≤ 11, -15 ≤ l ≤ 15	-11 ≤ h ≤ 12, -11 ≤ k ≤ 11, -15 ≤ l ≤ 13
R_{int}	0.0400	0.0340	0.0433
Reflections collected/unique	5877/1002	15133/1771	15400/1794
GOF on F^2	1.107	1.143	1.077
Flack factor	0.00	-	-
R_1/wR_2 [$I > 2\sigma(I)$][a]	0.0353/0.0771	0.0235/0.0581	0.0398/0.1081
R_1/wR_2 (all data)	0.0400/0.0788	0.0281/0.0599	0.0473/0.1124
Largest diff. peak and hole (e Å^{-3})	1.583 and -0.703	0.957 and -0.869	1.108 and -2.496

[a] $R_1 = \sum||F_o| - |F_c||/\sum|F_o|$; $wR_2 = [\sum w(F_o^2 - F_c^2)^2]/\sum w(F_o^2)^2]^{1/2}$

2.6 Powder X-ray Diffraction (XRD). Powder XRD data of **1**−**3** were recorded on an automated Bruker D8 Advance X-ray diffractometer equipped with Cu-Kα

radiation (λ = 1.5418 Å) in the angular range 2θ = 5−70° with a scan step-width of 0.02°.

2.7 Scanning Electron Microscopy (SEM). The morphologies of **1**−**3** were investigated using scanning electronic microscopy (Hitachi S-4800, Japan) operating at 15 kV.

2.8 Infrared (IR) Spectroscopy. The IR spectra were measured on a Nicolet 360 FT-IR instrument within the range 500−4000 cm^{-1}. The samples were mixed thoroughly with dried KBr and were then pressed into discs for measurements.

2.9 Thermal Analysis. A TGA/1100SF instrument was used to analyze the thermal stabilities of the three compounds. The samples were heated from 30 °C to 900 °C with a heating rate of 15 °C/min in nitrogen gas.

2.10 UV-Vis-NIR Diffuse Reflectance Spectra. Optical diffuse-reflectance spectra were measured at room temperature with a UV-3600 Plus UV-Vis-NIR spectrophotometer. $BaSO_4$ was used as a standard. Reflectance spectra were converted into absorbance based on the Kubelka-Munk function [32].

2.11 Luminescent Measurements. The luminescent emission spectra were recorded by using a Cary Eclipse spectrofluorophotometer (Varian, America) at room temperature.

2.12 Second-Order NLO Measurements. The measurements of the powder frequency-doubling effects were performed at room temperature on the sieved samples by using the modified method of Kurtz and Perry [33] with laser radiation of

λ = 1064 nm generated by a Q-switched Nd:YAG solid-state laser. The crystal samples of **1** were ground and sieved into three distinct particle size ranges (<26, 50−74, and 105−150 μm), which were pressed into disks with diameters of 6 mm that were placed between glass microscope slides and secured with tape in a 1 mm thick aluminum holder.

3 RESULTS AND DISCUSSION

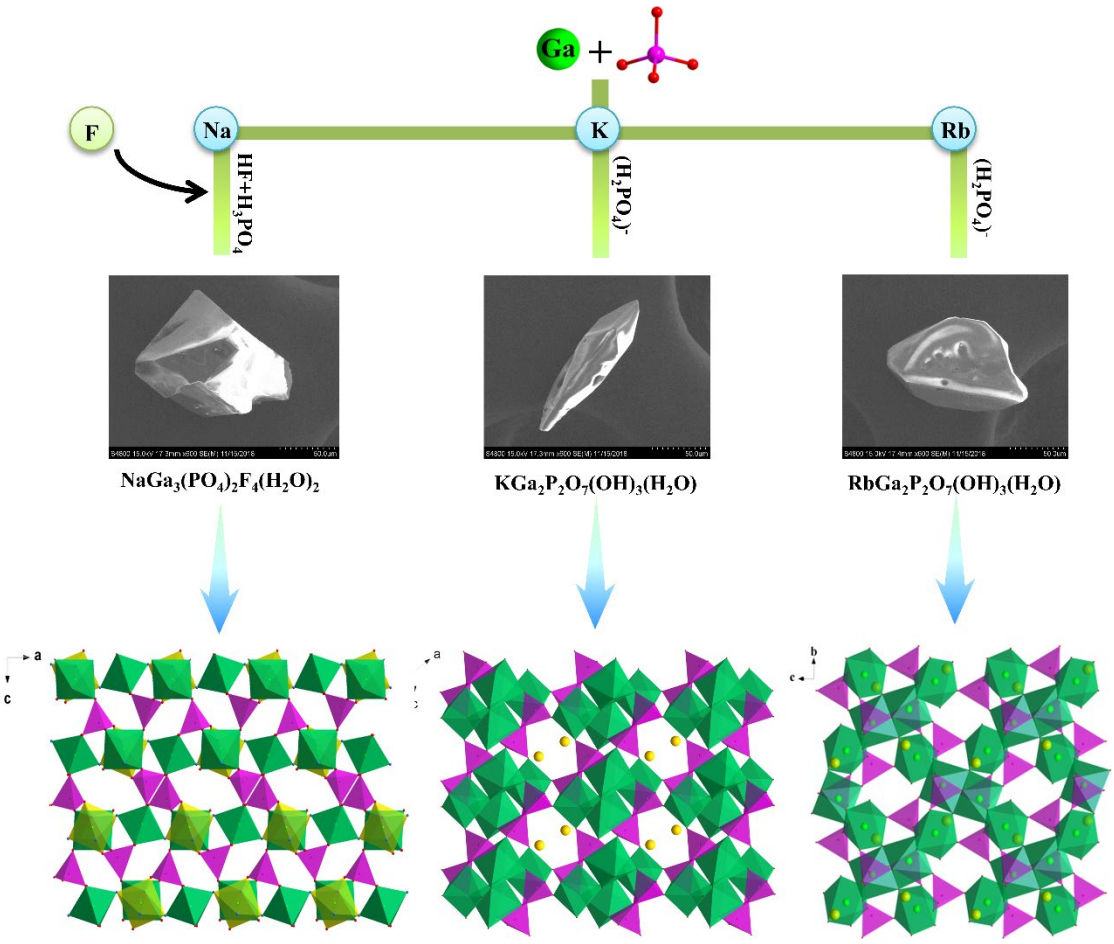

Scheme 1: The synthetic process and the structural features of **1**−**3**. Color codes: Na turquoise, K gold, Rb lime, Ga bright green, P pink, O red, F light blue, GaO_4F_2 octahedron green, GaO_2F_4 octahedron yellow, GaO_6 octahedron green, PO_4 tetrahedron pink.

3.1 Syntheses. Three types of crystals in the alkali-metal gallium phosphates system have been synthesized by employing different starting materials under hydrothermal conditions. The polycrystalline samples of **1**−**3** were synthesized through facile hydrothermal reactions based on the following chemical equations: $3GaO(OH) + Na^+ + 4F^- + 2H_3PO_4 \rightarrow NaGa_3(PO_4)_2F_4(H_2O)_2 + H_2O + 3OH^-$ for **1**, $2GaO(OH) + K^+ + 2(H_2PO_4)^- \rightarrow KGa_2P_2O_7(OH)_3(H_2O) + OH^-$ for **2**, and $2GaO(OH) + Rb^+ + 2(H_2PO_4)^- \rightarrow RbGa_2P_2O_7(OH)_3(H_2O) + OH^-$ for **3**. Scheme 1 summarizes the reaction conditions, SEM images and the structural features of **1**−**3**, including two isostructural compounds **2** and **3**. By using GaO(OH), H_3PO_4, and NaF as the starting materials, compound **1** was obtained as colorless block crystals in 48% yield (based on Ga). Employing GaO(OH), KCl/RbCl, and $(NH_4)(H_2PO_4)$ as the reaction materials afforded **2** and **3** as colorless block-like crystals in 50% yield and 43% (based on Ga), respectively. All three of these crystalline materials were stable under ambient conditions for several months.

Table 2 Reaction conditions and product phases of **1**−**3**.

No.	Composition of Reagent	Product phases
1	GaO(OH): NaF: H_3PO_4: HF	Block crystal **1**
2	GaO(OH): KF: H_3PO_4: HF	White powder **I**
3	GaO(OH): RbF: H_3PO_4: HF	White powder **II**
4	GaO(OH): CsF: H_3PO_4: HF	White powder **III**
5	GaO(OH): Na salt:[a] $(NH_4)(H_2PO_4)$	White powder **VI**
6	GaO(OH): K salt: $(NH_4)(H_2PO_4)$	Block crystal **2**
7	GaO(OH): Rb salt: $(NH_4)(H_2PO_4)$	Block crystal **3**
8	GaO(OH): Cs salt: $(NH_4)(H_2PO_4)$	White powder **V**

(a) Na salt denotes NaCl/$NaNO_3$/KF; the same as K/Rb/Cs salts.

It is well-known that the structures of phosphates are very sensitive to the synthetic conditions (including starting materials, reaction medium, pH, concentration of phosphates, reaction temperature, and reaction time) [1b]. In the present study, the starting materials play a key role in promoting the crystallization of the three phosphates. It is noticeable that during the hydrothermal procedure, small amounts of HF are necessary for the synthesis of **1**; this is favorable for improving the crystal quality. Similar experimental protocols and reaction conditions were assayed for the synthesis of other oxyfluorinated alkali-metal (K, Rb, Cs) gallium phosphates and alkali-metal (Na, Cs) gallium phosphates (Table 2), but all have been unsuccessful to date, suggesting that the cation size, reaction stoichiometry, and precise synthetic conditions may play crucial roles in the syntheses. The main component of white powder for reaction No. 2 is $KGaF_5 \cdot 2H_2O$, while the white powders for reaction No. 3 and No. 4 are some unknown phases because no matching compound can be isolated. With respect to reaction No. 5 and No. 8, the main component of white powder is $GaPO_4 \cdot 2H_2O$ (Figure S7).

3.2 Crystal Structures.

3.2.1 Crystal Structure of 1. $NaGa_3F_4(PO_4)_2(H_2O)_2$ crystallizes in chiral tetragonal space group $P4_32_12$ (No. 96). The FBUs for **1** contain GaO_4F_2, GaO_2F_4 (Figure 1a), NaO_8, PO_4 groups. Each GaO_2F_4 unit connects two adjacent GaO_4F_2 units by corner-sharing F(1) and F(2) atoms, forming novel infinite 1D chains along the *a*-axis, which can be described as alternating GaO_2F_4 (type A) and GaO_4F_2 (type B) units

with an ABABAB cyclization manner (Figure 1b). The 1D chains are further linked by GaO_4F_2 units to build a 2D layer in the *ab* plane with 8-membered rings (8-MRs) in which the Na cations are located (Figure 1c). Further connectivity of the layers, namely through PO_4 tetrahedra, yields a 3D framework with 7-MR channels and 6-MR channels along the *b*-axis (Figure 1d, 2a). The 7-MR consists of three GaO_4F_2 octahedra, two GaO_2F_4 octahedra, and two PO_4 tetrahedra, with Ga···Ga distances in the range of 5.53 Å−7.55 Å (Figure 2b). The 6-MR is built from three GaO_4F_2, one GaO_2F_4, and two PO_4 units, with Ga···Ga distances varying from 4.98 Å to 5.97 Å (Figure 2b).

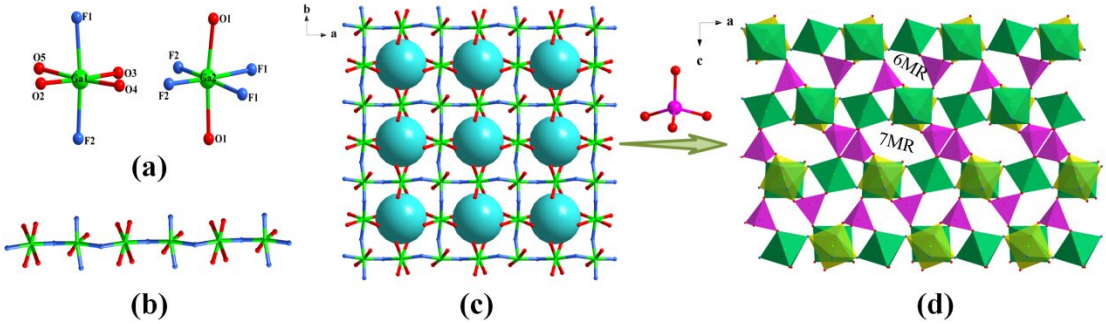

Figure 1. (a) The GaO_4F_2 and GaO_2F_4 octahedra in **1**. (b) View of the infinite chain constructed from GaO_4F_2 and GaO_2F_4 units. (c) View of the 2D layer in the *ab* plane with Na atoms locate in the 8MR. (d) View of the 3D structure of **1** along the *b*-axis showing the 7-MR and 6-MR channels. The Na−O bonds have been omitted for clarity. Color codes: Na turquoise, Ga bright green, P pink, O red, F light blue, GaO_4F_2 octahedron green, GaO_2F_4 octahedron yellow, PO_4 tetrahedron pink.

The asymmetric unit of **1** contains 1 Na, 2 Ga, 1 P, 5 O, and 2 F atoms. There are two unique Ga atoms. The Na atoms are in eight-coordinated environments, bonded to O atoms with Na−O bond distances in the range of 2.461(5)−2.789(6) Å. Ga(1) is coordinated to four O atoms and two F atoms to form a GaO_4F_2 octahedron, while Ga(2) coordinate to two O atoms and four F atoms in an octahedral manner. Ga(2) and

Na(1) atoms are located on the 4a special sites and the rest of atoms occupy the general sites. The Ga−O/F bond distances fall in the ranges 1.900(4)−2.077(5) Å and 1.920(4)−2.000(4) Å, respectively. Each P atom is tetrahedrally coordinated by four O atoms with P−O bond lengths and O−P−O bond angles ranging from 1.515(5)−1.549(5) Å and 107.2(3)−112.2(3)°, respectively. There are weak hydrogen bonds not only between O atoms and H_2O molecules but also between F atoms and H_2O molecules, with O···O/F distances of 2.758 Å and 2.917 Å, respectively (Table S4). Bond valence sum (BVS) calculations for atoms Na(1), Ga(1), Ga(2), and P(1) gave values of 1.15, 3.01, 2.86, and 4.90 (Table S7), respectively, consistent with oxidation states of +1 for Na, +3 for Ga, and +5 for P.

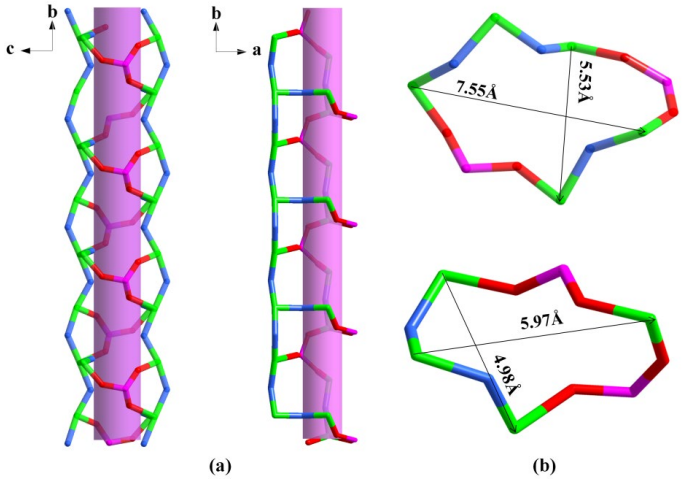

Figure 2. (a) View of the 7-MR (left) and 6-MR (right) channels in **1**. (b) The pore size of the 7-MR(top) and the 6-MR (down). Color codes: Na turquoise, Ga bright green, P pink, O red, F light blue.

We also compared the structure of **1** with that of $LiGa_3F_3(OH)(PO_4)_2(H_2O)_2$ [34] as they have the same Ga/P stoichiometry. There are two types of Ga atoms, GaO_4F_2 and GaO_3F_3 octahedra, in $LiGa_3F_3(OH)(PO_4)_2(H_2O)_2$, while in **1** the Ga atoms adopt two coordination modes in the GaO_4F_2 and GaO_2F_4 octahedra. In addition, the 2D

oxyfluorinated gallolayers of the two compounds are all constructed from 1D chains linked by GaO_4F_2 units, while the FBUs of the 1D chains varies. In the structure of $LiGa_3F_3(OH)(PO_4)_2(H_2O)_2$, the infinite chain is built from GaO_3F_3 units linked via corner-sharing mode, whereas the infinite chain in **1**, is composed of GaO_4F_2 and GaO_2F_4 connected by sharing common F atoms.

3.2.2 Crystal Structure of 2 and 3. Single-crystal X-ray diffraction analysis revealed that the two gallium phosphate crystals $AGa_2P_2O_7(OH)_3(H_2O)$ (A = K **2**, Rb **3**) are isostructural, both crystallizing in the orthorhombic crystal system with centrosymmetric space group $P2_1/c$ (No. 14); as a result, only a representative structure, that of crystal **2**, will be discussed in detail. In the gallium phosphate crystal, the FBU, Ga_4O_{20}, is composed of four GaO_6 octahedra (Figure 3a). Each Ga_4O_{20} unit is attached to adjacent eight FBUs via eight PO_4 units (Figure 3b). Further connectivity of the Ga_4O_{20} FBUs, namely through PO_4 units, yields a 3D anionic framework with 8-MR channels running along *b*-axis (Figure 3c, 4a), the diameters of the channel are about 7.12 × 6.25 $Å^2$ (Figure 4c). The K cations are located in the 8-MR channels (Figure 4b).

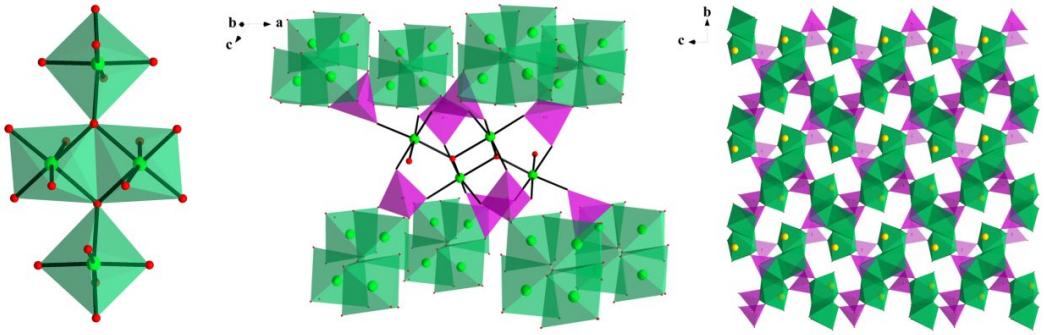

(a) **(b)** **(c)**

Figure 3. (a) The Ga_4O_{20} tetramer unit. (b) Perspective view of the Ga_4O_{20} tetramer unit link with eight FBUs projected along the *b*-axis. (c) View of the 3D framework of **2** along the *a*-axis. Color codes: K gold, Ga bright green, P pink, O red, GaO_6 octahedron green, PO_4 tetrahedron pink.

In each asymmetric unit of **2**, there is one K atom, two Ga atoms, two P atoms, and eleven O atoms. Atom K(1) in **2** is 10-coordinate and the K−O bond distances range from 2.780(4) Å to 3.543(4) Å. Ga(1) and Ga(2) are octahedrally coordinated. The Ga−O bond distances of the $Ga(1)O_6$ and $Ga(2)O_6$ groups are in the ranges 1.902(2)−2.120(2) Å and 1.909(3)−2.143(2) Å, respectively. The O−Ga−O angles fall in the ranges 84.12(11)−174.74(11)° for $Ga(1)O_6$ and 84.37(10)−178.13(10)° for $Ga(2)O_6$. P(1) and P(2) each coordinate to four O atoms in a tetrahedral manner. The P−O bond lengths and O−P−O bond angles are in the ranges of 1.515(3)−1.560(3) Å and 106.24(14)−112.84(15)°. These values are comparable to those previously reported gallium phosphate compounds [35]. In addition, there are weak hydrogen bonds between the H_2O molecules and the O atoms, with O···O distances varying from 2.771 Å to 3.024 Å (Table S5). The calculated total BVS are 0.95, 3.20, 3.07, 5.00, and 5.01 for K(1), Ga(1), Ga(2), P(1), and P(2) (Table S8), respectively, indicating that K, Ga, and P are in oxidation states of +1, +3, and +5, respectively.

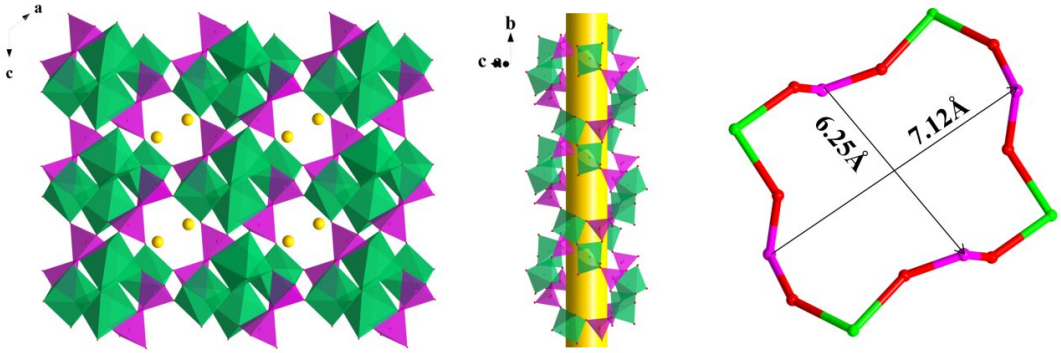

(a) (b) (c)

Figure 4. (a) Framework structure of **2** viewed along the *b*-axis showing the 8-MR channels. (b) View of the 8-MR channel in **2**. (c) The pore size of the 8-MR. Color codes: K gold, Ga bright green, P pink, O red, GaO_6 octahedron green, PO_4 tetrahedron pink.

The crystal structure of **2** is derived from the leucophosphite ($K[Fe_2(PO_4)_2(OH)(H_2O)]\cdot H_2O$) [36] structure type. In $K[Fe_2(PO_4)_2(OH)(H_2O)]\cdot H_2O$, the Fe_4O_{20} units are formed by a central pair of edge-sharing FeO_6 octahedra, to which two additional FeO_6 octahedra are attached by corner-sharing, corresponding to the Ga_4O_{20} tetramer in compound **2**. We also compared the structure of **2** with that of $NaGa_2(OH)(PO_4)_2$ [11] as they exhibit the same Ga/P stoichiometry. In $NaGa_2(OH)(PO_4)_2$, the Ga_4O_{18} tetrameter units are interconnected by the PO_4 tetrahedra into a 3D anionic framework. The comparison between the anionic framework of the two compounds clearly shows that the two kind of tetrameters varies. The Ga_4O_{20} tetrameter in compound **2** consists of four GaO_6 units, whereas the tetrameter in $NaGa_2(OH)(PO_4)_2$, is constructed by two GaO_6 units and two GaO_5 units. Both two types tetrameters adopt the same connecting manner as well as that in the leucophosphite.

3.3 X-ray Powder Diffraction. Powder XRD patterns of **1**−**3** were also obtained (Figure S5); there is a good match between the experimental powder XRD patterns of the three samples and the calculated ones derived from the single-crystal data, confirming bulk homogeneity of these materials.

3.4 IR Measurements. The infrared spectra of **1**−**3** are shown in Figure S6, and are comparable with reported metal gallium phosphates [9a]. The absorption peaks

around 3490 and 1640 cm^{-1} for **1**; 3457, 3325, and 1654 cm^{-1} for **2**; and 3475, 3364, and 1654 cm^{-1} for **3** are due to the H−O stretching and bending vibration. The strong absorption bands at 1061 cm^{-1} for **1**; 1101 and 1003 cm^{-1} for **2**; 1101 and 996 cm^{-1} for **3** are attributed to the stretching mode of P−O vibrations. The bands at 575 cm^{-1} for **1**; 601 and 560 cm^{-1} for **2**; and 627 and 561 cm^{-1} for **3** might be ascribed to the bending vibrations of the P−O−P bonds of PO_4 groups.

3.5 Thermal Stabilities. Thermalgravimetric analysis (TGA) for **1**−**3** are shown in Figure 5. The TGA curve of **1** reveals that it is thermally stable up to 400 ºC. It exhibits a small step of weight loss in the range of 400−500 ºC, which corresponds to the loss of two water molecules (found, 7.32%; calcd, 6.67%). The thermal behaviors

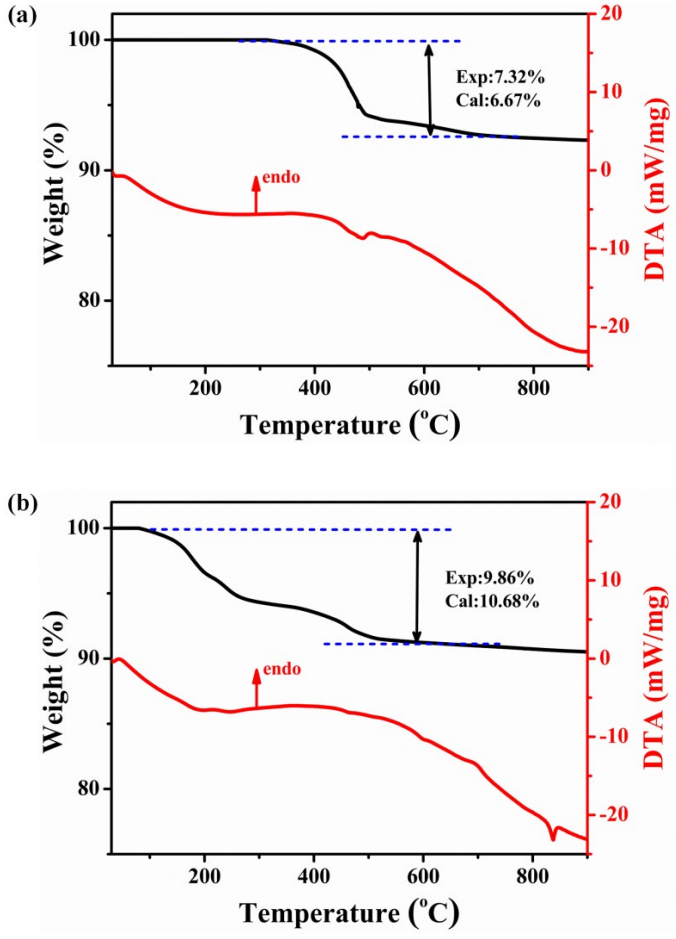

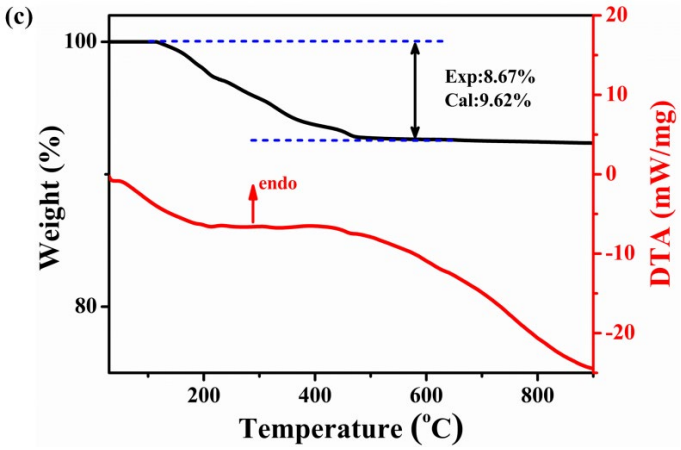

Figure 5. TGA-DTA curves of **1** (a), **2** (b), and **3** (c).

of **2** and **3** are almost the same. As shown in the TGA curves, both compounds are thermally stable up to 130 ºC. The weight loss step in the range of 130−500 ºC corresponds to the release of one H_2O molecular and dehydration of the hydroxyls per formula unit (found, 9.86% for **2** and 8.67% for **3**; calcd, 10.68% for **2** and 9.62% for **3**). The DTA curves of **2** and **3** are consistent with these. The final residuals of the three compounds were examined, but no matching compounds could be identified from the powder XRD patterns.

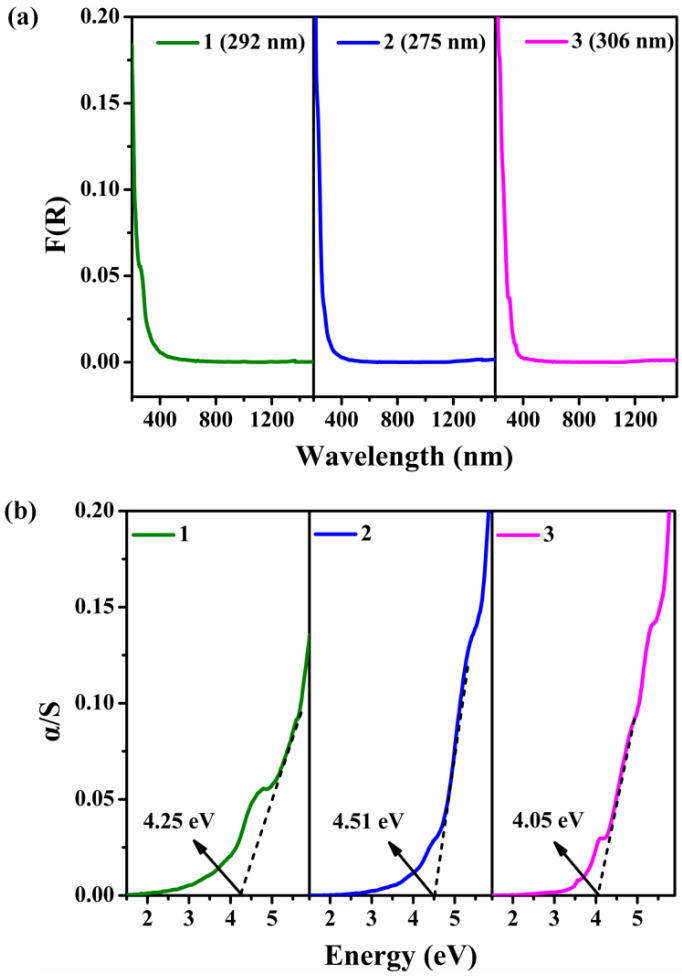

Figure 6. (a) UV-Vis-NIR diffuse reflectance spectra of **1**, **2**, and **3**. (b) The corresponding band gaps of **1**, **2**, and **3**.

3.6 UV-Vis-NIR Diffuse Reflectance Spectra. The UV-Vis-NIR diffuse reflectance spectra for **1**−**3** are shown in Figure 6. Absorption data were calculated employing the Kubelka-Munk function: $F(R) = (1-R)^2/2R = K/S$. **1**−**3** have wide band-gap energies of 4.25, 4.51 and 4.05 eV with cut-off edges of 292, 275 and 306 nm, respectively. The UV cut-off edges are at much shorter wavelengths than those of known hydrated phosphates, such as $Fe(IO_3)(HPO_4)(H_2O)$ (3.01 eV), $Sc(IO_3)(HPO_4)(H_2O)$ (3.56 eV), and $RbMgPO_4{\cdot}6H_2O$ (4.3 eV) [37,38]. The wide transparency range (from the UV to

the NIR) and short wavelength cut-off edges of **1**–**3** indicate that all three compounds have the potential for applications in the UV region.

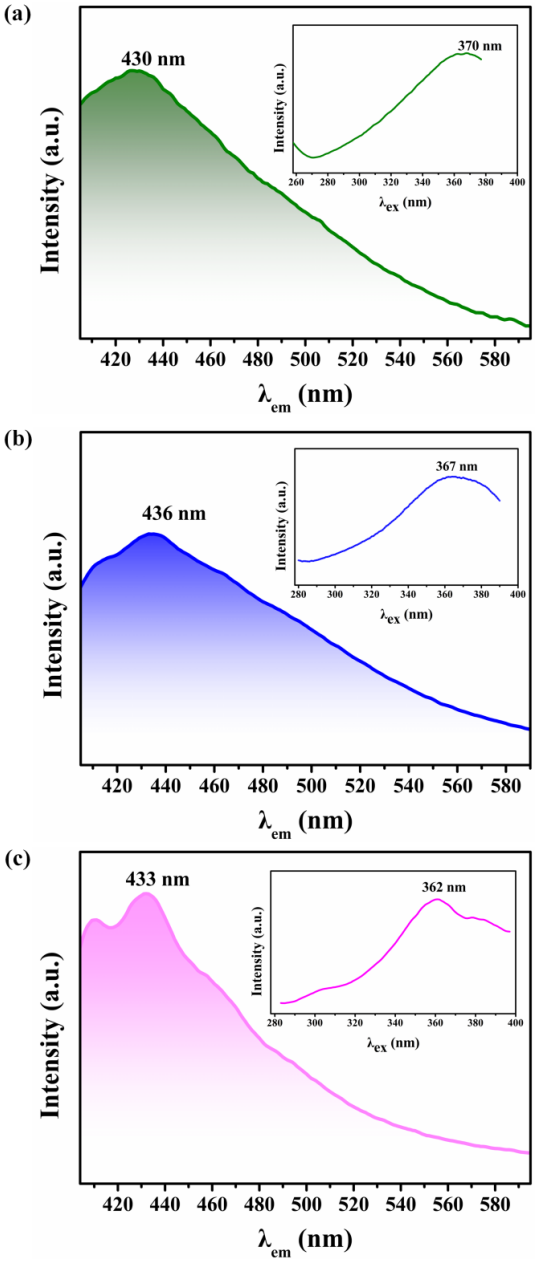

Figure 7. Solid state emission spectra of **1** (a), **2** (b), and **3** (c). The insets show the corresponding excitation spectra.

3.7 Luminescent properties. The luminescent properties of **1**–**3** were investigated in the solid state at room temperature. As shown in Figure 7, compounds **1**, **2**, and **3** exhibit blue luminescent peaks at 430 nm (λ_{ex} = 370 nm), 436 nm (λ_{ex} = 367 nm), and

433 nm (λ_{ex} = 362 nm), respectively. Since the emission energy of 2.88 (2.84, 2.86) eV is less than the cut-off edges of 4.25 (4.51, 4.05) eV for **1**–**3**, respectively, we can deduce that the emitted fluorescence probably originates from the defects or excitons [39]. Figure 8 demonstrates the commission international deL'Eclairage chromaticity diagram for the aforementioned three compounds. The color coordinate of the three compounds are (0.1781, 0.1916), (0.1765, 0.1976), and (0.1738, 0.1558), respectively. Interestingly, **1**–**3** exhibit blue emissions under the excitation of near-ultraviolet light, suggesting that they are potential phosphors and can be efficiently excited by near-ultraviolet chips.

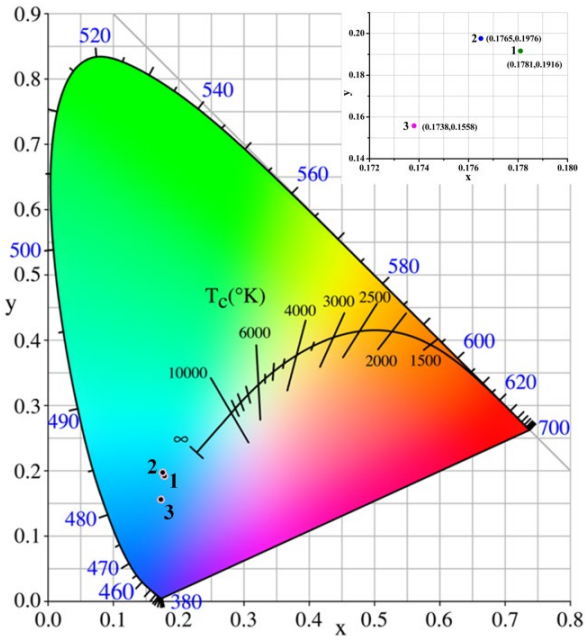

Figure 8. The Commission Internationale de I'Eclairage (CIE) chromaticity coordinates of **1**, **2**, and **3** excited with 370 nm, 367 nm, and 362 nm, respectively.

3.8 SHG Measurements. Compound **1** is located at NCS and chiral space group $P4_32_12$ (No. 96) and belongs to point group 422. The point group symmetry requires that two non-vanishing tensors of second-order susceptibility should be satisfied the

equation $d_{14} = -d_{25}$. However, on the basis of the restriction of Kleinman symmetry, d_{14} must be equal to d_{25}. Consequently, the two tensors d_{14} and d_{25} are zero. Therefore, any compound crystallizing in the point group 422 is forbidden from exhibiting an SHG response by Kleinman symmetry. Consistent with its assignment to the NCS space group ($P4_32_12$), compound **1** displays no SHG response when irradiated with 1064 nm laser light.

4 CONCLUSION

In summary, three new alkali-metal gallium phosphates, $NaGa_3F_4(PO_4)_2(H_2O)_2$ (**1**), $KGa_2P_2O_7(OH)_3(H_2O)$ (**2**), and $RbGa_2P_2O_7(OH)_3(H_2O)$ (**3**) have been synthesized by facile hydrothermal methods. Compound **1** crystallizes in the chiral space group $P4_32_12$. The structure of **1** features a three-dimensional (3D) framework composed of 2D layers of corner-sharing GaO_4F_2 and GaO_2F_4 octahedra that are further bridged by PO_4 tetrahedra with Na^+ cations residing in the oxyfluorinated gallolayers. Compounds **2** and **3** are isostructural, both crystallizing in the centrosymmetric space group $P2_1/c$; their structures consist of novel 3D gallium phosphate frameworks constructed from Ga_4O_{20} FBUs interconnected by PO_4 units with 8-membered ring channels along the *b*-axis, in which K^+/Rb^+ cations are located. The diffuse reflectance spectra show that the UV cut-off edges are about 292 nm (4.25 eV), 272 nm (4.51 eV), and 306 nm (4.05 eV) for **1**−**3**, respectively. Luminescent studies suggest that **1**−**3** emit blue light, suggesting that they are potential phosphors and can be efficiently excited by near-ultraviolet chips.

ACKNOWLEDGMENTS

This work was supported by the National Natural Science Foundation of China (No. 51432006 and 51172100), the Ministry of Education of China for the Changjiang Innovation Research Team (No. IRT13R24), and the Ministry of Education and the State Administration of Foreign Experts Affairs for the 111 Project (No. B13025), the Innovation Program of Shanghai Municipal Education Commission, and the National and Shanghai Postdoctoral Program for Innovative Talents (nos. BX201800216 and 2018192).

Appendix A. Supplementary material

Electronic supplementary information (ESI) available: selected bond distances and angles, Hydrogen-bonding interactions, Atomic coordinates, equivalent isotropic displacement parameters, and bond valence calculations, additional structures, simulated and measured powder XRD patterns, IR spectra. X-ray crystallographic file in CIF format (CCDC-1892695 for **1,** CCDC-1892696 for **2,** and CCDC-1892709 for **3**).

References

1 (a) C. Wu, G. Yang, M. G. Humphrey, C. Zhang, Recent advances in ultraviolet and deep-ultraviolet second-order nonlinear optical crystals, *Coord. Chem. Rev.* 375 (2018) 459-488. (b) R. Murugavel, A. Choudhury, M. G. Walawalkar, R. Pothiraja, C. N. R. Rao, Metal complexes of organophosphate esters and open-framework metal phosphates: synthesis, structure, transformations, and applications, *Chem. Rev.* 108 (2008) 3549-3655. (c) J. Jiang, J. Yu, A. Corma, Extra-large-pore zeolites: bridging the gap between micro and mesoporous structures, *Angew. Chem. Int. Ed.* 49 (2010) 3120-3145.

2 (a) P. Shi, H. Zheng, X. Liang, Y. Sun, S. Cheng, C. Chen, H, Xiang, A highly concentrated phosphate-based electrolyte for high-safety rechargeable lithium batteries, *Chem. Commun.* 54 (2018) 4453-4456. (b) D. Wang, X. Bie, Q. Fu, D. Dixon, N. Bramnik, Y. S. Hu, F. Fauth, Y. Wei, H. Ehrenberg, G. Chen, F. Du, Sodium vanadium titanium phosphate electrode for symmetric sodium-ion batteries with high power and long lifespan, *Nat. Commun.* 8 (2017) 15888. (c) C. Karegeya, A. Mahmoud, B. Vertruyen, F. Hatert, R. P. Hermann, R. Cloots, F. Boschini, One-step hydrothermal synthesis and electrochemical performance of sodium-manganese-iron phosphate as cathode material for Li-ion batteries, *J. Solid State Chem.* 253 (2017) 389-397.

3 (a) J. Qiao, L. Ning, M. S. Molokeev, Y. C. Chuang, Q. Liu, Z. Xia, Eu^{2+} site preferences in the mixed cation $K_2BaCa(PO_4)_2$ and thermally stable luminescence, *J. Am. Chem. Soc.* 140 (2018) 9730-9736. (b) D. Zhao, J. Zhao, Y. L. Xue, B. F. Hu, X. Xin, Y. C. Fan, B. Z. Liu, A new diphosphate $Li_2Na_2P_2O_7$: synthesis, crystal structure, electronic structure and luminescent properties, *J. Solid State Chem.* 269 (2019) 125-131. (c) M. Chen, Z. Xia, M. S. Molokeev, C. C. Lin, C. Su, Y. C. Chuang, Q. Liu, Probing Eu^{2+} luminescence from different crystallographic sites in $Ca_{10}M(PO_4)_7$:Eu^{2+} (M = Li, Na, and K) with β-$Ca_3(PO_4)_2$-type structure, *Chem. Mater.* 29 (2017) 7563-7570. (d) Y. M. Mao, Y. Zhang, L. Li, J. Li, H. M. Zeng, G. H. Zou, Z. E. Lin, Crystalline metal phosphates with layered structures: Synthesis, luminescence, and proton conduction. *J. Solid State Chem.* 282 (2020) 121067.

4 (a) J. Lu, J. N. Yue, L. Xiong, W. K. Zhang, L. Chen, L. M. Wu, Uniform alignment of non-π-conjugated species enhances deep ultraviolet optical nonlinearity. *J. Am. Chem. Soc.* 141 (2019) 8093-8097. (b) J. Chen, L. Xiong, L. Chen, L. M. Wu, $Ba_2NaClP_2O_7$: unprecedented phase matchability induced by symmetry breaking and its unique fresnoite-type structure, *J. Am. Chem. Soc.* 140 (2018) 14082-14086. (c) L. Kang, M. Zhou, J. Yao, Z. Lin, Y. Wu, C. Chen, Metal thiophosphates with good mid-infrared nonlinear optical performances: a first-principles prediction and analysis, *J. Am. Chem. Soc.* 137 (2015) 13049-13059. (d) Z. Xie, X. Su, H. Ding, H. Li, Crystal structures and theoretical studies of polyphosphate $LiZnP_3O_9$ for nonlinear optical applications, *J. Solid State Chem.* 262 (2018) 313-319. (e) C. Wu, L. Li, G. Yang, J. Song, B. Yan, M. G. Humphrey, L. Zhang, J. Shao, C. Zhang, Low-temperature-flux syntheses of ultraviolet transparent borophosphates $Na_4MB_2P_3O_{13}$ (M = Rb, Cs) exhibiting a second-harmonic generation response, *Dalton Trans.* 46 (2017) 12605-12611. (f) L. J. Huang, J. Li, H. M. Zeng, G. H. Zou, Y. Zhao, L. Huang, J. Bi, D. J. Gao, Z. E. Lin, Surfactant-thermal synthesis of amino acid-templated zinc phosphates with 3-connected nets related to zeolite ABW. *Inorg. Chem.* 58 (2019) 4089-4092.

5 (a) J. Jiang, S. Lee, B. Zhu, Y. Yu, J. C. Waerenborgh, K. Y. Choi, M. Lu, Variable dimensionality, valence, and magnetism in fluoride-rich iron phosphates $Ba_xFe_x(PO_4)F_y$ ($1 \leq x \leq 3$, $2 \leq y \leq 12$), *Inorg. Chem.* 58 (2019) 133-142. (b) V. D. Zhuravlev, D. G. Kellerman, A. P. Tyutyunnic, A. Y. Chufarov, R. F. Samigullina, Synthesis, structure and magnetic properties of new γ-$Ba(CoV_{1-x}P_xO_4)_2$ x = 0.4-0.5, *J. Solid State Chem.* 266 (2018) 174-180. (c) M. Usman, G. Morrison, V. V. Klepov, M. D. Smith, H. C. Loye, Flux crystal growth, structure, magnetic and optical properties of a family of alkali uranium(IV) phosphates, *J. Solid State Chem.* 270 (2019) 19-26.

6 (a) Y. J. Liu, M. G. Kanatzidis, Postintercalative polymerization of aniline and its derivatives in layered metal phosphates, *Chem. Mater.* 7 (1995) 1525-1533. (b) P. Yu, L. M. Wu, L. J. Zhou, L. Chen, Deep-ultraviolet nonlinear optical crystals: $Ba_3P_3O_{10}X$ (X = Cl, Br), *J. Am. Chem. Soc.* 136 (2014) 480-487.

7 (a) Y. J. Liu, M. G. Kanatzidis, Topotactic polymerization of aniline in layered uranyl phosphate, *Inorg. Chem.* 32 (1993) 2989-2991. (b) S. Volkov, M. Petrova, O. Sinel'shchikova, V. Firsova, V. Popova, V. Ugolkov, M. Krzhizhanovskaya, R. Bubnova, Crystal structure and thermal properties of the $Li_xNa_{1-x}KZnP_2O_7$ solid solutions and its relation to the MM' ZnP_2O_7 diphosphate family *J. Solid State Chem.* 269 (2019) 486-493.

8 (a) M. J. Sie, C. H. Lin, S. L. Wang, Polyamine-cladded 18-ring-channel gallium phosphites with high-capacity hydrogen adsorption and carbon dioxide capture, *J. Am. Chem. Soc.* 138 (2016) 6719-6722. (b) F. Hamchaoui, V. Alonzo, I. Marlart, S. Auguste, C. Galven, H. Rebbah, E. L. Fur, Hydrothermal synthesis, structural and thermal characterizations of three open-framework gallium phosphites, *J. Solid State Chem.* 255 (2017) 8-12. (c) Z. Yan, C. W. Kirby, Y. Huang, Characterization of the gel phases formed in the synthesis of microporous gallophosphate, cloverite, *J. Mater. Chem.* 20 (2010) 10200-10210.

9 (a) J. Wu, C. Tao, Y. Li, J. Li, J. Yu, Methyl viologen-templated zinc gallophosphate zeolitic material with dual photo-/thermochromism and tuneable photovoltaic activity, *Chem. Sci.* 6 (2015) 2922-2927. (b) F. Gao, L. Huang, Y. Ma, S. Jiao, Y. Jiang, Y. Bi, Ionothermal synthesis, characterization of a new layered gallium phosphate with an unusual heptamer SBU, *J. Solid State Chem.* 254 (2017) 155-159. (c) N. Syed, A. Zavabeti, J. Z. Ou, M. Mohiuddin, N. Pillai, B. J. Carey, B. Y. Zhang, R. S. Datta, A. Jannat, F. Haque, K. A. Messalea, C. Xu, S. P. Russo, C. F. Mcconville, T. Daeneke, K. K. Zadeh, Printing two-dimensional gallium phosphate out of liquid metal *Nat. Commun.* 9 (2018) 3618.

10 (a) C. Tao, J. Wu, Y. Yan, C. Shi, J. Li, A new methylviologen-templated zinc gallophosphate zeolite with photo-/thermochromism, fluorescent and

photoelectric properties, *Inorg. Chem. Front.* 3 (2016) 541-546. (b) X. F. Fu, L. C. Lei, J. Q. Yang, L. H. Gao, Y. B. Wang, L. L. Liu, X. L. Yuan, H. Y. Liang, R. Sun, Y. Z. Liu, C. L. Qin, The ionothermal synthesis and properties of new gallium phosphates substituted by Co and Fe, *Polyhedron* 155 (2018) 129-134. (c) C. H. Lin, Y. C. Yang, C. Y. Chen, S. L. Wang, Unequivocal heteroatom insertion into a 24-ring channel gallophosphate and its photoluminescence, *Chem. Mater.* 18 (2006) 2095-2101.

11 A. Guesdon, Y. Monnin, B. Raveau, A sodium gallophosphate with an original tunnel structure: $NaGa_2(OH)(PO_4)_2$, *J. Solid State Chem.* 172 (2003) 237-242.

12 K. H. Lii, $Rb_2[Ga_4(HPO_4)(PO_4)_4]\cdot 0.5H_2O$: a new gallium phosphate containing four-, five, and six-coordinated gallium atoms, *Inorg. Chem.* 35 (1996) 7440-7442.

13 J. Lesage, A. Guesdon, M. Hervieu, B. Raveau, Unusual mobility of cesium via a reversible topotactic dehydration reaction in a new hydroxygallophosphate with an intersecting tunnel structure, *Chem. Mater.* 18 (2006) 2895-2903.

14 L. Beitone, N. Guillou, F. Millange, T. Loiseau, G. Ferey, Structural characterizations of lithium gallium phosphates, analogous to the amblygonite-montebrasite series, *Solid State Sci.* 4 (2002) 1061-1065.

15 J. Lesage, A. Guesdon, B. Raveau, $RbGa_3(P_3O_{10})_2$: a new gallium phosphate isotypic with $RbAl_3(P_3O_{10})_2$, *Acta. Cryst.* C61 (2005) i44-i46.

16 D. Sun, R. Cao, Y. Sun, W. Bi, M. Hong, A novel open-framework gallium phosphate containing two different building units, *Eur. J. Inorg. Chem.* 2003 1303-1305.

17 (a) Y. Wang, B. Zhang, Z. Yang, S. Pan, Cation-tuned synthesis of fluorooxoborates: towards optimal deep-ultraviolet nonlinear optical materials, *Angew. Chem. Int. Ed.* 57 (2018) 2150-2154. (b) G. Shi, Y. Wang, F. Zhang, B. Zhang, Z. Yang, X. Hou, S. Pan, K. R. Poeppelmeier, Finding the next deep-ultraviolet nonlinear optical material: $NH_4B_4O_6F$, *J. Am. Chem. Soc.* 139 (2017) 10645-10648. (c) X. Huang, B. Liu, R. C. Zhuang, Y. Pan, J. X. Mi, Y. X. Huang, Multiple fluorine-substituted phosphate germanium fluorides and their thermal stabilities, *Inorg. Chem.* 55 (2016) 12376-12382.

18 (a) S. Zhao, X. Yang, Y. Yang, X. Kuang, F. Lu, P. Shan, Z. Sun, Z. Lin, M. Hong, J. Luo, Non-centrosymmetric $RbNaMgP_2O_7$ with unprecedented thermo-induced enhancement of second harmonic generation, *J. Am. Chem. Soc.* 140 (2018) 1592-1595. (b) B. L. Ellis, W. R. M. Makahnouk, Y. Makimura, K. Toghill, L. F. Nazar, A multifunctional 3.5 V iron-based phosphate cathode for rechargeable batteries, *Nat. Mater.* 6 (2007) 749-753. (c) X. Fu, W. Lu, M. Jiao, H. You, Broadband yellowish-green emitting $Ba_4Gd_3Na_3(PO_4)_6F_2:Eu^{2+}$ phosphor: structure refinement, energy transfer, and thermal stability, *Inorg. Chem.* 55 (2016) 6107-6113.

19 Y. Feng, J. Huang, L. Liu, J. Liu, X. Yu, Rare-earth-free white emitting $Ba_2TiP_2O_9$ phosphor: revealing its crystal structure and photoluminescence properties, *Dalton Trans.* 44 (2015) 11554-11559.

20 (a) M. Amer, P. Boutinaud, The doping sites in Eu^{2+}-doped $A^IB^{II}PO_4$ phosphors and their consequence on the photoluminescence excitation spectra, *J. Solid State Chem.* 258 (2018) 124-130. (b) J. Olchowka, O. Mentre, H. Kabbour, M. Colmont, M. Adlung, M. Suta, C. Wickleder, Bonding scheme and optical properties in $BiM_2O_2(PO_4)$ (M=Cd, Mg, Zn); experimental and theoretical analysis, *Chem. Eur. J.* 23 (2017) 15694-15703.

21 (a) C. Wu, L. Li, J. Song, G. Yang, M. G. Humphrey, C. Zhang, Facile syntheses of $Ba_2[B_4O_7(OH)_2]$ and $Na[B_5O_7(OH)_2](H_2O)$ borate salts exhibiting nonlinear optical activity in the ultraviolet, *Inorg. Chem.* 56 (2017), 1340-1348. (b) C. Wu, L. Lin, X. X. Jiang, Z. S. Lin, Z. P. Huang, M. G. Humphrey, C. Zhang, $K_5(W_3O_9F_4)(IO_3)$: an efficient mid-infrared nonlinear optical compound with high laser damage threshold. *Chem. Mater.* 31 (2019) 10100-10108. (c) C. Wu, L. H. Li, L. Lin, Z. P. Huang, M. G. Humphrey, C. Zhang, $K_5(W_3O_9F_4)(IO_3)$: an efficient mid-infrared nonlinear optical compound with high laser damage threshold. *Chem. Mater.* (2020) DOI: 10.1021/acs.chemmater.0c00034. (d) C. Wu, L. H. Li, L. Lin, Z. P. Huang, M. G. Humphrey, C. Zhang, $Gd(NO_3)(Se_2O_5)\cdot 3H_2O$: a nitrate–selenite nonlinear optical material with a short ultraviolet cutoff edge. *Dalton Trans.* 49 (2020) 3253-3259.

22 Z. Xiao, Y. Sun, Y. X. Bao, Y. Sun, R. Zhou, L. Wang, Two new inorganic-organic hybrid zinc phosphate frameworks and their application in fluorescence sensor and photocatalytic hydrogen evolution, *J. Solid State Chem.* 269 (2019) 575-579.

23 M. Li, V. Smetana, M. W. Kozubek, Y. Mudryk, T. Alammar, V. K. Pecharsky, A. V. Mudring, Open-framework manganese(II) and cobalt(II) borophosphates with helical chains: structures, magnetic, and luminescent properties, *Inorg. Chem.* 56 (2017) 11104-11112.

24 H. L. Huang, Y. T. Huang, S. L. Wang, A crystalline mesolamellar gallium phosphate with zwitterionic-type templates exhibiting green afterglow property, *Inorg. Chem.* 55 (2016) 6836-6838.

25 H. Yu, J. Young, H. Wu, W. Zhang, J. M. Rondinelli, P. S. Halasyamani, $M_4Mg_4(P_2O_7)_3$ (M = K, Rb): structural engineering of pyrophosphates for nonlinear optical applications, *Chem. Mater.* 29 (2017) 1845-1855.

26 Y. Shen, Y. Yang, S. Zhao, B. Zhao, Z. Lin, C. Ji, L. Li, P. Fu, M. Hong, J. Luo, Deep-ultraviolet transparent Cs_2LiPO_4 exhibits an unprecedented second harmonic generation, *Chem. Mater.* 28 (2016) 7110-7116.

27 B. Zhang, G. Han, Y. Wang, X. Chen, Z. Yang, S. Pan, Expanding frontiers of ultraviolet nonlinear optical materials with fluorophosphates, *Chem. Mater.* 30 (2018) 5397-5403.

28 Y. C. Yang, S. L. Wang, Intrinsic yellow light phosphor: an Organic-Inorganic hybrid gallium oxalatophosphate with hexameric octahedral $Ga_6(OH)_4O_{26}$ cluster, *J. Am. Chem. Soc.* 130 (2008) 1146-1147.

29 (a) B. H. Lei, Z. Yang, H. Yu, C. Cao, Z. Li, C. Hu, K. R. Peoppelmeier, S. Pan, Module-guided design scheme for deep-ultraviolet nonlinear optical materials, *J. Am. Chem. Soc.* 140 (2018) 10726-10733. (b) A. Guesdon, Y. Monnin, B. Raveau, A new sodium hydroxygallophosphate containing tetrameric gallium units: $Na_3[Ga_4O(OH)(H_2O)(PO_4)_4]\cdot H_2O$, *J. Solid State Chem.* 177 (2004) 181-188.

30 G. M. Sheldrick, SHELXS-97: Program for the Solution of Crystal Structures, University of Gottingen, Germany, 1997. (b) G. M. Sheldrick, SHELXS-97: Program for the Refinement of Crystal Structures, University of Gottingen, Germany, 1997.

31 A. L. Spek, Single-crystal structure validation with the program PLATON. *J. Appl. Crystallogr.* 36 (2013) 7-13.

32 W. M. Wendlandt, H. G. Hecht, Reflectance Spectroscopy, Interscience, New York, 1966.

33 S. K. Kurtz, T. T. Perry, A powder technique for the evaluation of nonlinear optical materials, *J. Appl. Phys.* 39 (1968) 3798-3813.

34 L. Beitone, J. Marrot, C. Lorentz, F. Taulelle, T. Loiseau, G. Ferey, Hydrothermal synthesis and structure determination of the first three-dimensional oxyfluorinated gallium phosphate incorporating lithium, *Solid State Sci.* 3 (2001) 641-647.

35 P. Ramaswamy, S. Mandal, S. Natarajan, New open-framework phosphate and phosphite compounds of gallium, *Inorg. Chim. Acta.* 372 (2011) 136-144.

36 S. Dick, T. Zeiske, Leucophosphite $K[Fe_2(PO_4)_2(OH)(H_2O)]\cdot H_2O$: hydrogen bonding and structural relationships, *J. Solid State Chem.* 133 (1997) 508-515.

37 T. Y. Chang, B. P. Yang, C. L. Hu, D. Yan, J. G. Mao, $M(IO_3)(HPO_4)(H_2O)$ (M = Sc, Fe, Ga, In): introduction of phosphate anions into metal iodates, *Cryst. Growth Des.* 17 (2017) 4984-4989.

38 Y. Zhou, L. Cao, C. Lin, M. Luo, T. Yan, N. Ye, W. Cheng, $AMgPO_4\cdot 6H_2O$ (A = Rb, Cs): strong SHG responses originated from orderly PO_4 groups, *J. Mater. Chem. C* 4 (2016) 9219-9226.

39 T. Y. Chang, C. L. Hu, D. Yan, J. G. Mao, $(H_3O)Ca_2Zn_{3.5}(PO_4)_4$ and $Ba_2Cd_3(PO_4)_2(HPO_4)_2$: syntheses, crystal structures and characterizations of two mixed metal phosphates, *J. Solid State Chem.* 251 (2017) 19-25. (b) X. A. Chen, K. Wang, X. A. Chang, W. Q. Xiao, Syntheses and characterization of two alkaline and transition metal orthoborates, $LiMBO_3$ (M = Zn, Cd), *Solid State Sci.* 52 (2016) 132-140.